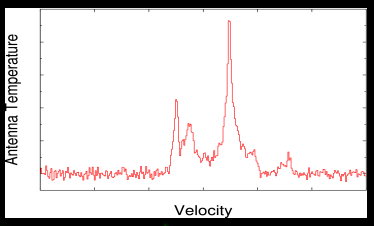

Herschel Open Time Key Programme:

Galactic Observations of Terahertz C^+: GOT C+

User Provided Data Release Document
21 January 2017

William D. Langer
Jet Propulsion Laboratory, California Institute

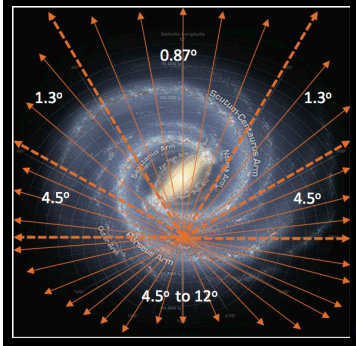

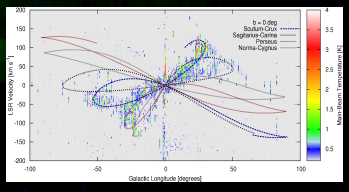

Herschel Open Time Key Programme:
Galactic **O**bservations of **T**erahertz **C**$^+$ (**GOT C+**)

User Provided Data Products Release Notes

W. D. Langer, P. F. Goldsmith, J. L. Pineda, and T. Velusamy
Jet Propulsion Laboratory, California Institute of Technology, 4800 Oak Grove Dr., Pasadena, CA 91109

This document briefly describes science data products delivered to the *Herschel Science Center* (HSC) for the User Provided Data Products (UPDP) from the *Herschel* Open Time Key Programme (KPOT_wlanger_1), "State of the Diffuse ISM: Galactic Observations of Terahertz C$^+$ (**GOT C+**)", whose P.I. is W. D. Langer. These data also include observations from the *Herschel* Performance Verification Phase (PVP) and Priority Science Program (PSP). The GOT C+ Programme consisted of (i) a Galactic plane survey of HIFI [C II] pointed observations towards 150 longitude directions; and, (ii) and on-the-fly [C II] scan maps of the Central Molecular Zone (CMZ) consisting of two on-the-fly strip scans through (l,b) =(0º,0º). In 2013 we delivered the data for the Galactic disk survey and in 2016 the CMZ scan maps. This document has been updated to include information on the CMZ data products.

1. Overview and Goals of the [C II] Galactic Plane Survey

The scientific goal of the **GOT C+** program was to understand the properties of the interstellar medium (ISM) containing ionized carbon. The observational technique employed was to survey the Galactic Plane in the 157.74 μ (1.90054 THz) fine-structure $^2P_{3/2} \rightarrow {}^2P_{1/2}$ transition of C$^+$, hereafter [C II], with sufficient spectral resolution to identify individual gas components. The [C II] line is an important tracer of the interstellar gas including the warm ionized medium (WIM), the cold neutral medium (CNM), the CO-dark H_2 clouds, and the photon dominated regions (PDRs) of dense molecular clouds. The use of high spectral resolution is driven by the need to characterize the gas properties using the spectral line properties: main beam temperature, linewidth, and integrated intensity to determine column density, kinetic temperature, and/or density of the gas, and dynamical state, while the velocity of the peak can be used, along with a rotation curve for the Galaxy, to locate the source.

Carbon, the fourth most abundant element in the Universe, is important for tracing the ISM gas because its main gaseous forms: carbon ions (C$^+$), atomic carbon (C), and carbon monoxide (CO), readily emit at temperatures and densities characteristic of many of the ISM's components, and are thus not only gas diagnostics, but important coolants. Figure 1 shows an energy and transition diagram for [C II] along with the two fine structure lines of neutral carbon, [C I], and the lowest seven rotational lines of CO. While large scale spectrally resolved surveys have been made of the Galactic diffuse atomic hydrogen gas via observation of the 21-cm HI line, and that of molecular hydrogen in the UV-shielded portions of molecular clouds with surveys of its primary tracer the CO (J=1→0) line, much less is known on a Galactic scale about the location and characteristics of the phase where the hydrogen is molecular, but there is little or no CO due to photodissociating far-UV (FUV) radiation.

GOT C+ conducted the first large-scale Galactic plane survey of spectrally resolved [C II]. The data were obtained with the *Herschel Space Observatory* (Pilbratt et al., 2010), using HIFI, the Heterodyne Instrument for the Far Infrared (de Graauw et al. 2010). **GOT C+** is a sparse survey containing several hundred lines of sight of spectrally resolved [C II] emission throughout the Galactic Disk covering longitudes $l = 0^o$ to 360^o mainly at five latitudes: $b = 0^o$, $\pm 0.5^o$, and $\pm 1.0^o$. The sampling in Galactic longitude is non-uniform in order to weight uniformly, as best as possible, the Galactic mass, with an emphasis on the important inner $l = 0^o$ to $\pm 90^o$. The **GOT C+** survey allows for a statistical approach to characterizing the ISM with [C II] by analyzing a large sample of spectrally resolved components dispersed throughout the Galaxy, rather than large scale maps of a few clouds. The **GOT C+** survey, while a very undersampled image compared to those produced by HI and CO surveys, reveals the association of [C II] emission with various Galactic cloud categories and their environments when used in conjunction with H I and CO observations. The reader can find more information about the **GOT C+** Galactic Plane survey and scientific results in the following papers published by the team: Langer et al. (2010), Pineda et al. (2010), Velusamy et al. (2010), Velusamy et al. (2012), Pineda et al. (2013), Langer et al. (2014), and Pineda et al. (2014). The latter three papers contain the most recent information on observations, data reduction, analysis, and scientific results of the [C II] survey. For [C II] excitation modeling and radiative transfer see Goldsmith et al. (2012) and for the latest in collisional rate coefficients see Wiesenfeld & Goldsmith (2014).

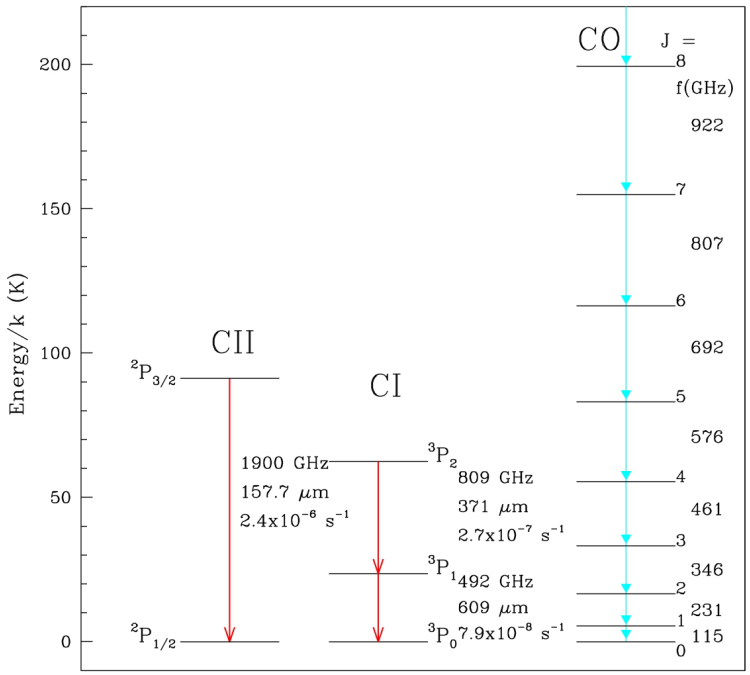

Figure 1. Shown are energy level diagrams for the fine structure lines of [C II] and [C I], and the first eight rotational levels of CO. The fine structure states are indicated along with the transition wavelengths, frequencies, and Einstein A coefficients. For CO, the rotational J levels are shown along with just the transition frequencies. [C II] is an efficient emitter only in warm ISM gas, typically $T_{kin} >$ 30-35K, as its upper level, $^2P_{3/2}$, is at an energy equivalent to 91.21K.

2. Galactic Plane [C II] Spectra

2.1 Sampling and Coverage

The **GOT C+** Galactic plane survey contains 454 lines of sight (LOS) at about 150 Galactic longitudes distributed throughout the disk. The sampling in Galactic longitude is every 0.87° for $|l| < 60°$, 1.3° for $30° < |l| < 60°$, and 4.5° for $60° < |l| < 90°$. In the Outer Galaxy, $|l| > 90°$, the observations were taken with a spacing starting with 4.5° and increasing to 13.5° as the longitude approaches $l = 180°$. At each longitude, there are observations either at Galactic latitude $b = 0.0°$, b=+0.5°, and +1.0° or at $b = 0.0°$, b= -0.5° and -1.0°. The observations at $|b|$ =0.5° and 1° were made at alternate positions in l. This alteration in l maximized the volume of the plane surveyed within the allotted observing time. At 22 longitudes in the Outer Galaxy with $|l| > 90°$ **GOT C+** also sampled at $|b| = 0°$, 1.0°, and 2.0° instead of at 0°, 0.5° and 1.0°.

2.2. Observing Mode

Here we briefly summarize the observing mode adopted for the **GOT C+** disk survey. The reader is referred to the HIFI Observers' Manual version 2.4 located on the Herschel Science Centre website (under HIFI documentation) for a detailed description of the HIFI instrument, its operational states, and observing modes.

The observations were taken using the two orthogonal linearly polarized receivers in band 7b, designated H- and V-polarization, using the wide-band spectrometer (WBS) with a channel resolution of 0.0788 km s^{-1}. The observations along a line of sight, designated the ON position, were made in the LoadChop mode using the optional OFF calibration reference mode. In the LoadChop mode an internal cold calibration source is used as a reference to correct short-term changes in the instrument behavior. This mode is useful when there are no emission-free regions that are near enough to be used as a reference position, which is an important consideration for [C II] with its potential for widespread emission. However, with the LoadChop mode alone there may remain a residual standing wave structure because the optical path differs between source and internal reference. To correct for this wave structure, we used a sky reference position, the OFF position, and corrected for [C II] contamination in the OFF position, as discussed below. To facilitate the correction for [C II] contamination in the OFF position, we used one fixed reference (OFF) position for a set of latitudes as follows: for a given Galactic longitude, lines of sight at $b = 0°$, +0.5° and +1.0° share the same reference position at b=+2° and for $b = 0°$, -0.5° and -1.0° they share the same reference position at b=-2°. The integration times on the OFF positions are three times that for each on position because the OFF position is common for all three b values at each longitude. In the Outer Galaxy, there are positions where we also observed $b = \pm 2.0°$, in these cases we used $b = \pm 4.0°$ as a reference for $b = \pm 2.0°$, respectively, and then used the processed observations at $b = \pm 2.0°$ as a reference for $b = 0°$ and $\pm 1.0°$.

2.3. Data Reduction

The [C II] 1.9THz observations were carried out with both the H- and V-polarization receivers. Each polarization was reduced separately in the pipeline and then combined in CLASS in the final steps. The data reduction is shown schematically in Figure 2 as a flow diagram. The steps are ordered as follows and the corresponding numbers given in Figure 2.

1) We processed the ON and OFF data with the HIPE 8 pipeline using the standing wave removal option HEBBaselineFit to produce the [ON-OFF] spectrum. The HEB bands in HIFI show prominent electrical standing waves that are produced between the HEB mixing element and the first low noise amplifier. The standing wave shape is not a regular sinusoid and is difficult to remove from the resulting spectrum using standard fitting methods (Higgins & Kooi 2009). To remove these standing waves, we used HEBBaselineFit, a procedure developed at the HIFI Instrument Control Center (ICC; Ian Avruch, private communication) that generates a library of standing wave shapes from different observations and finds the one that best corresponds to the observed baseline to correct the observed spectrum (see Higgins 2011 for a detailed description of this method).

2) We also processed the [ON] position without the OFF subtraction step in the HIPE8 pipeline, in order to determine the [OFF] position spectrum for examination of any emission in the OFF position. However, for position switch mode, because of the way that HIPE8 works, it is not possible to reduce just the OFF spectrum.

3) We removed the residual electrical standing waves for the [ON-OFF] spectrum and the [ON] spectrum by fitting a single sinusoidal function using the fitHIFIFringe procedure.

4) After all electrical standing waves are removed, we exported the [ON-OFF] data to the CLASS90 data analysis software (www.iram.fr/IRAMFR/GILDAS), in order to combine different polarizations, apply a main-beam efficiency of 0.72 to transform the data from an antenna temperature to a main-beam temperature scale (Roelfsema et al. 2012), boxcar average over ten channels resulting in a velocity resolution of 0.79 km s^{-1}, and remove the baseline with a polynomial fit (typically of order 3) For this channel width the average rms noise of our data is $\sim$ 0.1K.

5) To determine the emission in the [OFF] position we extracted the [OFF] spectrum by performing the following operation: [OFF] =-{[ON-OFF] – [ON]}. The [OFF] spectrum was processed in CLASS similarly to that for the [ON-OFF] spectrum described in step (4) above, with one additional operation. The [OFF] spectra include a standing wave with period ~90 MHz, which was removed with a Fast Fourier Transform (FFT). There are usually six OFF observations at each longitude (3 *b* positions and 2 polarizations) and we combined all of them in CLASS to improve the signal-to-noise in the [OFF] position.

6) We decomposed the [OFF] spectral emission into Gaussian components (at a latitude of $\pm 2.0^{\circ}$, there are generally few spectra in any passband). Roughly 50% of the **GOT C+** spectra were corrected for emission in the reference position.

7) The final step was to add the [OFF] spectral components to the [ON] spectrum to produce the final [C II] spectrum.

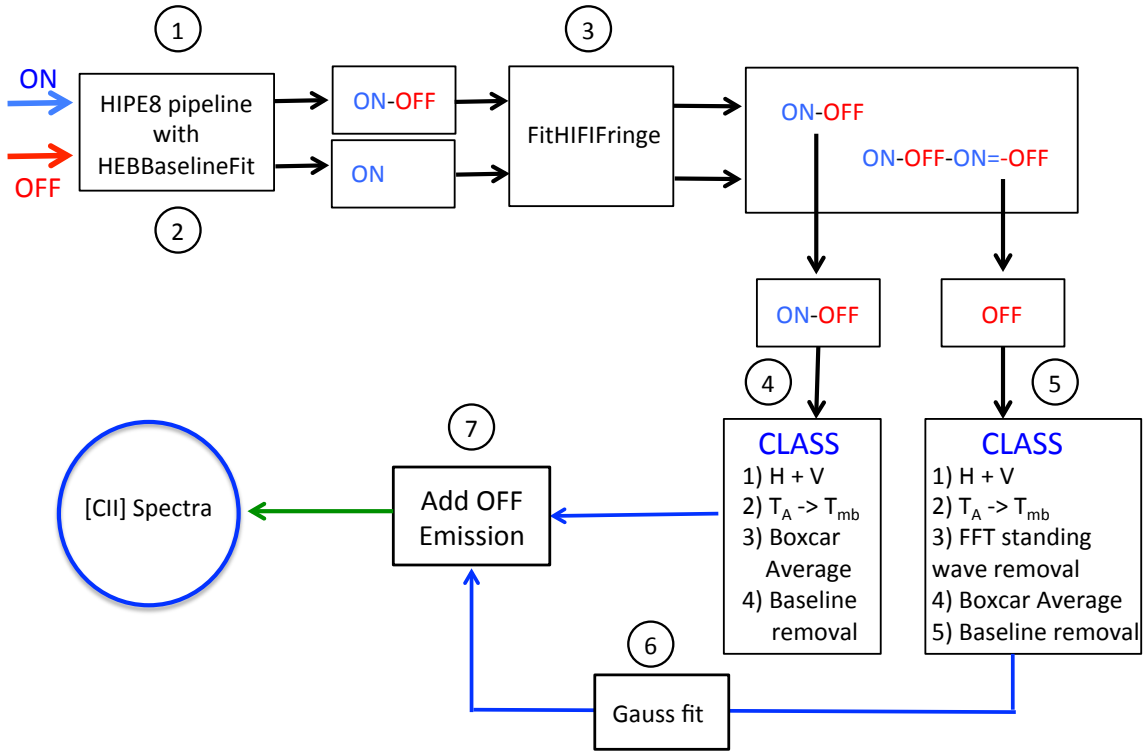

Figure 2. A flow diagram of the seven steps in reducing the **GOT C+** [C II] data for the ON and reference OFF positions. The numbers inside the circles correspond to each of the steps in the text.

In Figure 3 we show examples of the [C II] spectra along four lines of sight, including one longitude at all three values of latitude, *b*; the spectra are labeled with their LOS-IDs as defined below in Section 4.

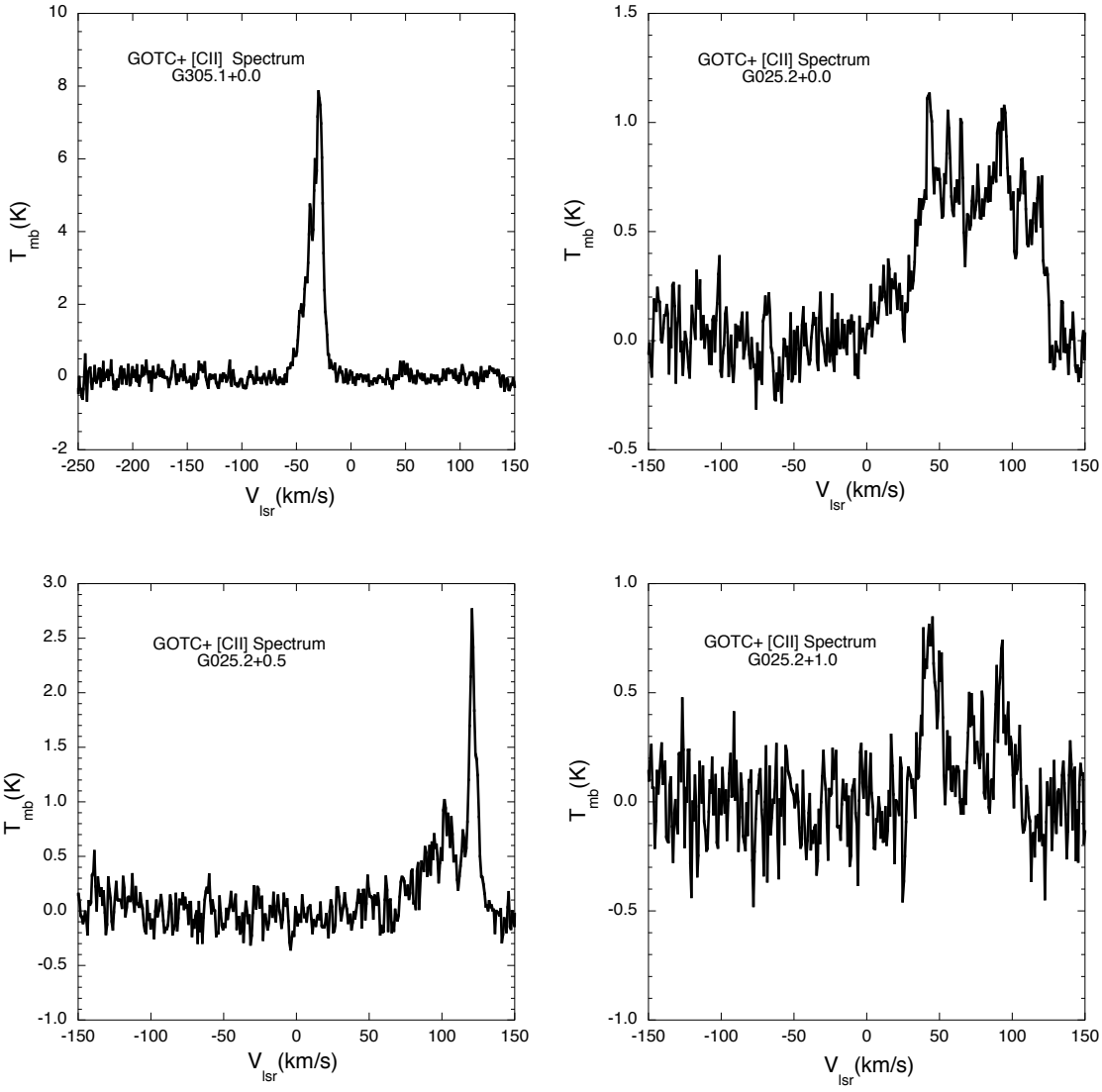

Figure 3. The reduced [CII] spectra are shown at four positions labeled with their LOS-ID (see Section 4). The upper left is towards the Galactic Center (l,b)=(0°,0°), while the others show examples of the spectra along G025.2 for three values of latitude, b=0.0°, 0.5°, and 1.0°.

2.4 Data Product

The final reduced spectra for this data release are in the form of ASCII files and can be found in the folder: GOTC+_[CII]_Galactic_Plane_Survey. The reduced data for each line of sight has a unique identification label, LOS-ID, in the following format: GXXX.X+Z.Z, where the first term gives the longitude, *l*, rounded off to one decimal place, and the second the latitude, *b*, in degrees. Each data file also contains a header with information about the observations, including the observing mode, the Galactic latitude, GLAT, to three decimal places, the Galactic longitude, GLON, the Herschel observation identification numbers, OBSIDs, and two columns, the first gives the LSR Velocity in km/s and the second is the [C II] Main Beam Temperature, T_{mb}, in Kelvins. The Header has the following information and format:

```
# PROPOSAL KPOT_wlanger_1 GOT C+
# INSTRUMENT/MODE HIFI/LOAD CHOP
# [CII] SPECTRUM AT:
# GLON       xxx.xxx
# GLAT       y.y
# OBSID001   xxxxxxxx
# OBSID002   yyyyyyyy
…….
# COLUMN1  LSR VELOCITY [km/s]
# COLUMN2  MAIN BEAM TEMPERATURE [K]
```

A sample data file is given below showing the header and a partial list of data values for G334.3+-0.5:

```
# PROPOSAL KPOT_wlanger_1 GOT C+
# INSTRUMENT/MODE HIFI/LOAD-CHOP
# [CII] SPECTRUM AT:
# GLON  334.348
# GLAT  -0.5000
# OBSID001 1342205742
# COLUMN1  LSR_VELOCITY [km/sec]
# COLUMN2  MAIN BEAM TEMPERATURE [K]
-302.16058349609 0.610478
-301.37185668945 0.462689
-300.58316040039 0.00800094
-299.79446411133 0.206514
-299.00576782227 0.194074
…
…
…
97.712615966797  0.277008
98.501319885254  0.0797409
99.290023803711  0.117238
100.07872772217 -0.021973
100.86743164062  0.0849617
101.65613642764 -0.196474
```

In Table 1 (below) and in the archive Lookup Table, we list all observed positions with the LOS-ID, exact longitude and latitude used for the pointing, and the OBSIDs. We refer the reader interested in reconstructing the spectra, or wanting additional details about the observations, including the reference positions, to the *Herschel* OBSIDs.

3. Central Molecular Zone Strip Scans

The **GOT C+** on-the-fly strip scans in the Central Molecular Zone (CMZ) are discussed in Langer et al. (2017), where the reader can find details on the observations, data reduction, and results, as well as many useful references. The CMZ is a roughly 400 pc by 100 pc region stretching from $l\sim$ -1° to $\sim$ +1.5° that is a significantly different environment than the Galactic disk. Among many prominent features in the CMZ are a massive black hole, the Galactic Center Bubble containing the Arches and Quintuplet clusters, the Radio Arc and Arched Filaments, and gas streams of dense molecular clouds orbiting the Galactic Center at a radius of 100 to 120 pc. The CMZ molecular clouds contain about 10% of the Galaxy's molecular gas, have high average densities, reside in a high thermal pressure environment, are relatively densely packed and have regions with an intense flux of stellar Far-UV radiation as well as X-rays. The CMZ produces about 10% of the Galaxy's infrared luminosity.

The CMZ's interstellar medium has been fully or partially mapped spectrally in over twenty mainly neutral gas tracers, or dense ion trace molecules. However, these species do not trace all the major components of the inner Galaxy, where the gas is highly ionized or where the UV irradiated neutral gas is weakly ionized. These regions include the Photon Dominated Regions (PDRs), the ionized boundary layers (IBL) surrounding UV-irradiated molecular clouds, HII regions, CO-dark H_2 clouds, and the warm and diffuse ionized gas. Less is known about these components due to the difficulty of observing key tracers of the ionized gas, the fine structure lines of C^+ and N^+, from the ground. The **GOT C+** CMZ strip scans, using the spectrally resolved fine structure line of ionized carbon, was a first step in characterizing the [C II] emission across the CMZ.

We observed the [C II] line using HIFI in an OTF mode to produce position-velocity maps of the Galactic center region. We observed two strip scans through $(l,b) = (0°, 0°)$, one along longitudes from l =359.20° to 0.80° at latitude b=0° and the other strip scan along b= -0.80° to +0.80° at longitude l = 0°. Details of the observations and data reduction are given in Sections 2.1 and 2.2 of Langer et al. (2017). In Figure 4 we show the **GOT C+** [C II] position-velocity strip scan maps (Langer et al. 2017 Figure 2).

The CMZ 1.6° long longitudinal and latitudinal strip scans are stored as FITS files in the *Herschel* User Provided Data Products. Each of these strip scans is constructed from 8 individual strip scans of 24 arcmin length, and composed of two LO settings (to accommodate the full velocity range of [C II] emission). In Table 2 (below) we list all 16 of the 24 arcmin strip scans, including: 1) Target name; 2) Scan direction (latitude or longitude), 3) the (l,b) values for the center of scan, 4) the length of the scan in arcmin, 5) the OBSID, and, 6) the LO used. We refer the reader interested in reconstructing the spectra, or wanting additional details about the observations, including the reference positions, to the *Herschel* OBSIDs.

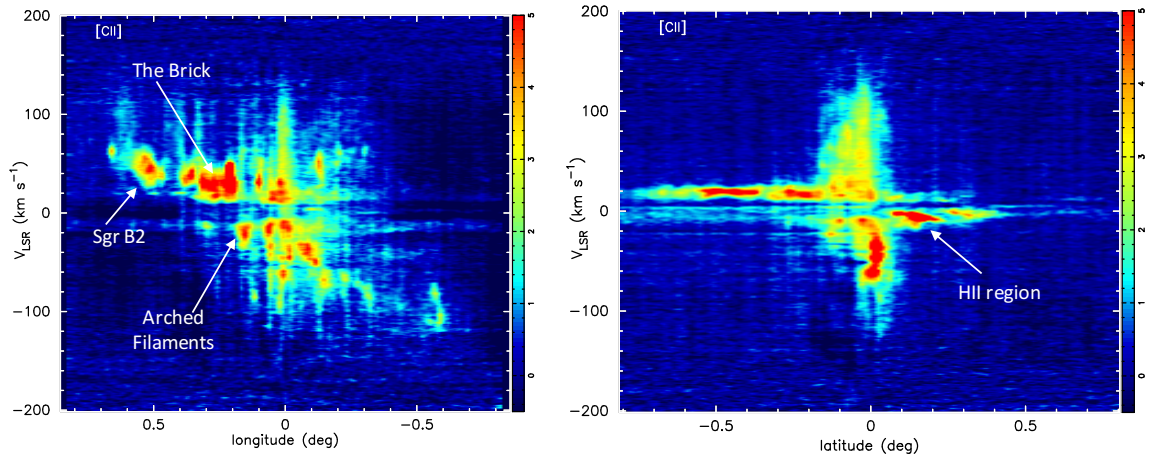

Figure 4. HIFI position-velocity [CII] maps of the CMZ tracing several notable features, including the Brick, Sgr B2, and the Arched Filaments. (left) The [CII] longitude-velocity map, *l*-*V*, covering 1.6° centered at (0°,0°). The color bar indicates the [CII] main beam temperature, T_{mb}(K). The vertical striations are artifacts of the baseline uncertainties (see Langer et al. (2017) Section 2). (right) The [CII] latitude-velocity map, *b*-*V*, covering 1.6 centered at (0°,0°). The color bar indicates T_{mb}([CII]) in degrees K. The arrow indicates a very bright [CII] peak that is likely a local foreground HII source and not from the CMZ.

4. Acknowledgments

The **GOT C+** data analysis team (W. D. Langer, P. F. Goldsmith, J. L. Pineda, and T. Velusamy) thanks the staffs of the ESA and the NASA Herschel Science Centers for their invaluable help with the data reduction routines. This work was performed at the Jet Propulsion Laboratory, California Institute of Technology, under contract with the National Aeronautics and Space Administration. ©2016 California Institute of Technology. Government sponsorship acknowledged.

5. References and Published Results with Additional Information

de Graauw, T., Helmich, F. P., Phillips, T. G., et al. 2010, A&A, 518, L6.

Goldsmith, P. F., Langer, W. D., Pineda, J. L., & Velusamy, T. 2012, ApJS, 203, 13.

Goldsmith, P. F., Yildiz, U., Langer, W. D., & Pineda, J. L., 2015, ApJ, 814, 133.

Higgins, D. R. 2011, Ph.D. Thesis, National University of Ireland Maynooth.

Higgins, R. D., & Kooi, J. W. 2009, in SPIE Conf. Ser., 7215.

Langer, W. D., Velusamy, T., Pineda, J. L., et al. 2010, A&A, 521, L17.

Langer, W. D., Velusamy, T., Pineda, J. L., Willacy, K., & Goldsmith, P. F. 2014, A&A, 561, A122.

Langer, W. D., Goldsmith, P. F., Pineda, J. L., Velusamy, T., Requena-Torres, M. A., Wiesemeyer, H., 2016, A&A, 590, A43.

Langer, W. D., Velusamy, T., Morris, M. R., Goldsmith, P. F., & Pineda, J. L., 2017, A&A, in press: ArXiv e-prints 1701.03482.

Ott, S., Bakker, J., Brumfitt, J., et al. 2006, in Astronomical Data Analysis Software and Systems XV, eds. C. Gabriel, C. Arviset, D. Ponz, & S. Enrique, ASP Conf. Ser. 351, 516.

Pilbratt, G. L., Riedinger, J. R., Passvogel, T., et al. 2010, A&A, 518, L1.

Pineda, J. L., Langer, W. D., Velusamy, T., & Goldsmith, P. F. 2013, A&A, 554, A103.

Pineda, J. L., Velusamy, T., Langer, W. D., et al. 2010, A&A, 521, L19.

Pineda, J. L., Langer, W. D., & Goldsmith, P. F., 2014, A&A, 570, A121.

Roelfsema, P. R., Helmich, F. P., Teyssier, D., et al. 2012, A&A, 537, A17.

Velusamy, T., Langer, W. D., Pineda, J. L., et al. 2010, A&A, 521, L18.

Velusamy, T., Langer, W. D., Pineda, J. L., & Goldsmith, P. F. 2012, A&A, 541, L10.

Velusamy T., Langer, W. D., Goldsmith, P. F., & Pineda, J. L., 2014, A&A, 578, A135.

Wiesenfeld, L. & Goldsmith, P. F. 2014, ApJ, 780, 183.

Table 1
Summary of Observed Lines of Sight in the Galactic Plane and Corresponding OBSIDs

LOS-ID	l(°)	b(°)	OBSID	OBSID	OBSID	OBSID
G000.0+0.0	0.0000	0.0	1342216780	1342216778	1342216777	1342216776
G000.0-0.5	0.0000	-0.5	1342216754	1342216753		
G000.0+0.5	0.0000	0.5	1342216775	1342216774		
G000.0+2.0	0.0000	2.0	1342216798	1342216797		
G000.5+0.0	0.5000	0.0	1342216794	1342216784	1342216773	1342216772
G000.9+0.0	0.8696	0.0	1342216751	1342216748		
G000.9+0.5	0.8696	0.5	1342216791	1342216788		
G000.9-0.5	0.8696	-0.5	1342216752	1342216750		
G000.9+1.0	0.8696	1.0	1342216790	1342216789		
G000.9-1.0	0.8696	-1.0	1342217669	1342216749		
G001.7+0.0	1.7391	0.0	1342214471	1342214470		
G001.7+0.5	1.7391	0.5	1342214473	1342214472		
G001.7+1.0	1.7391	1.0	1342214475	1342214474		
G002.6+0.0	2.6087	0.0	1342217668	1342217664		
G002.6-0.5	2.6087	-0.5	1342217667			
G002.6-1.0	2.6087	-1.0	1342218099	1342217666	1342217665	
G003.5+0.0	3.4783	0.0	1342217671			
G003.5+0.5	3.4783	0.5	1342217672			
G003.5+1.0	3.4783	1.0	1342217670			
G004.3+0.0	4.3478	0.0	1342218098			
G004.3-0.5	4.3478	-0.5	1342217663			
G004.3-1.0	4.3478	-1.0	1342217662			
G005.2+0.0	5.2174	0.0	1342217674			
G005.2+0.5	5.2174	0.5	1342217673			
G005.2+1.0	5.2174	1.0	1342217675			
G006.1+0.0	6.0870	0.0	1342218089	1342217676		
G006.1-0.5	6.0870	-0.5	1342218088	1342218087		
G006.1-1.0	6.0870	-1.0	1342218090	1342218086		
G007.0+0.0	6.9565	0.0	1342217678			
G007.0+0.5	6.9565	0.5	1342217677			
G007.0+1.0	6.9565	1.0	1342217679			
G007.8+0.0	7.8261	0.0	1342218084			
G007.8-0.5	7.8261	-0.5	1342218082			
G007.8-1.0	7.8261	-1.0	1342218083			
G008.7+0.0	8.6957	0.0	1342217680			
G008.7+0.5	8.6957	0.5	1342217681			
G008.7+1.0	8.6957	1.0	1342217682			

LOS-ID	l(°)	b(°)	OBSID	OBSID	OBSID	OBSID
G009.6+0.0	9.5652	0.0	1342218079			
G009.6-0.5	9.5652	-0.5	1342218081			
G009.6-1.0	9.5652	-1.0	1342218080			
G010.4+0.0	10.4348	0.0	1342218078	1342217684		
G010.4+0.5	10.4348	0.5	1342218077	1342217685		
G010.4+1.0	10.4348	1.0	1342217683			
G011.3+0.0	11.3043	0.0	1342218076			
G011.3-0.5	11.3043	-0.5	1342218075			
G011.3-1.0	11.3043	-1.0	1342218074			
G012.2+0.0	12.1739	0.0	1342218070	1342218069		
G012.2+0.5	12.1739	0.5	1342218068	1342218067		
G012.2+1.0	12.1739	1.0	1342218066			
G013.0+0.0	13.0435	0.0	1342218073			
G013.0-0.5	13.0435	-0.5	1342218072			
G013.0-1.0	13.0435	-1.0	1342218071			
G013.9+0.0	13.9130	0.0	1342218065			
G013.9+0.5	13.9130	0.5	1342218064			
G013.9+1.0	13.9130	1.0	1342218063			
G014.8+0.0	14.7826	0.0	1342218513	1342218512		
G014.8-0.5	14.7826	-0.5	1342218511	1342218510		
G014.8-1.0	14.7826	-1.0	1342218509			
G015.7+0.0	15.6522	0.0	1342218062			
G015.7+0.5	15.6522	0.5	1342218061			
G015.7+1.0	15.6522	1.0	1342218060			
G016.5+0.0	16.5217	0.0	1342218508	1342218507		
G016.5-0.5	16.5217	-0.5	1342218506	1342218505		
G016.5-1.0	16.5217	-1.0	1342218504			
G017.4+0.0	17.3913	0.0	1342218059			
G017.4+0.5	17.3913	0.5	1342218058			
G017.4+1.0	17.3913	1.0	1342218057			
G018.3+0.0	18.2609	0.0	1342218503	1342194766		
G018.3-0.5	18.2609	-0.5	1342218502	1342194765		
G018.3-1.0	18.2609	-1.0	1342194767			
G019.1+0.0	19.1304	0.0	1342218056			
G019.1+0.5	19.1304	0.5	1342218055			
G019.1+1.0	19.1304	1.0	1342218054			
G020.0+0.0	20.0000	0.0	1342218501			
G020.0-0.5	20.0000	-0.5	1342218500			
G020.0-1.0	20.0000	-1.0	1342208546			
G020.9+0.0	20.8696	0.0	1342218499			

LOS-ID	l(°)	b(°)	OBSID	OBSID	OBSID	OBSID
G020.9+0.5	20.8696	0.5	1342218498			
G020.9+1.0	20.8696	1.0	1342218497			
G021.7+0.0	21.7391	0.0	1342208547			
G021.7-0.5	21.7391	-0.5	1342208548			
G021.7-1.0	21.7391	-1.0	1342208549			
G022.6+0.0	22.6087	0.0	1342194758			
G022.6+0.5	22.6087	0.5	1342218496			
G022.6+1.0	22.6087	1.0	1342194757			
G023.5+0.0	23.4783	0.0	1342208551	1342194770		
G023.5-0.5	23.4783	-0.5	1342208553	1342194768		
G023.5-1.0	23.4783	-1.0	1342194769			
G024.3+0.0	24.3478	0.0	1342208557	1342194771		
G024.3+0.5	24.3478	0.5	1342208554	1342194772		
G024.3+1.0	24.3478	1.0	1342194773			
G025.2+0.0	25.2174	0.0	1342208558			
G025.2-0.5	25.2174	-0.5	1342208560			
G025.2-1.0	25.2174	-1.0	1342208559			
G026.1+0.0	26.0870	0.0	1342208563			
G026.1+0.5	26.0870	0.5	1342208562			
G026.1+1.0	26.0870	1.0	1342208561			
G027.0+0.0	26.9565	0.0	1342208564			
G027.0-0.5	26.9565	-0.5	1342208565			
G027.0-1.0	26.9565	-1.0	1342208566			
G027.8+0.0	27.8261	0.0	1342208569			
G027.8+0.5	27.8261	0.5	1342208568			
G027.8+1.0	27.8261	1.0	1342208567			
G028.7+0.0	28.6957	0.0	1342208570			
G028.7-0.5	28.6957	-0.5	1342218495			
G028.7-1.0	28.6957	-1.0	1342219523			
G030.0+0.0	30.0000	0.0	1342208571			
G030.0+0.5	30.0000	0.5	1342208573			
G030.0+1.0	30.0000	1.0	1342208572			
G031.3+0.0	31.2766	0.0	1342219522			
G031.3-0.5	31.2766	-0.5	1342219520			
G031.3-1.0	31.2766	-1.0	1342219521			
G032.6+0.0	32.5532	0.0	1342219518			
G032.6+0.5	32.5532	0.5	1342219517			
G032.6+1.0	32.5532	1.0	1342219516			
G033.8+0.0	33.8298	0.0	1342219508			
G033.8-0.5	33.8298	-0.5	1342219507			

LOS-ID	l(°)	b(°)	OBSID	OBSID	OBSID	OBSID
G033.8-1.0	33.8298	-1.0	1342219506			
G035.1+0.0	35.1064	0.0	1342219504			
G035.1+0.5	35.1064	0.5	1342219503			
G035.1+1.0	35.1064	1.0	1342219502			
G036.4+0.0	36.3830	0.0	1342219480			
G036.4-0.5	36.3830	-0.5	1342219478			
G036.4-1.0	36.3830	-1.0	1342219479			
G037.7+0.0	37.6596	0.0	1342219482			
G037.7+0.5	37.6596	0.5	1342219501			
G037.7+1.0	37.6596	1.0	1342219481			
G038.9+0.0	38.9362	0.0	1342219485			
G038.9-0.5	38.9362	-0.5	1342219483			
G038.9-1.0	38.9362	-1.0	1342219484			
G040.2+0.0	40.2128	0.0	1342219500			
G040.2+0.5	40.2128	0.5	1342219498			
G040.2+1.0	40.2128	1.0	1342219499			
G041.5+0.0	41.4894	0.0	1342219488			
G041.5-0.5	41.4894	-0.5	1342219487			
G041.5-1.0	41.4894	-1.0	1342219486			
G042.8+0.0	42.7660	0.0	1342219495			
G042.8+0.5	42.7660	0.5	1342219497			
G042.8+1.0	42.7660	1.0	1342219496			
G044.0+0.0	44.0426	0.0	1342219491			
G044.0-0.5	44.0426	-0.5	1342219489			
G044.0-1.0	44.0426	-1.0	1342219490			
G045.3+0.0	45.3191	0.0	1342219494			
G045.3+0.5	45.3191	0.5	1342219493			
G045.3+1.0	45.3191	1.0	1342219492			
G046.6+0.0	46.5957	0.0	1342219336			
G046.6-0.5	46.5957	-0.5	1342219335			
G046.6-1.0	46.5957	-1.0	1342219337			
G047.9+0.0	47.8723	0.0	1342219339			
G047.9+0.5	47.8723	0.5	1342219338			
G047.9+1.0	47.8723	1.0	1342219334			
G049.1+0.0	49.1489	0.0	1342220473			
G049.1-0.5	49.1489	-0.5	1342219326			
G049.1-1.0	49.1489	-1.0	1342219327			
G050.4+0.0	50.4255	0.0	1342220477			
G050.4+0.5	50.4255	0.5	1342220476			
G050.4+1.0	50.4255	1.0	1342220475			

LOS-ID	l(°)	b(°)	OBSID	OBSID	OBSID	OBSID
G051.7+0.0	51.7021	0.0	1342210176			
G051.7-0.5	51.7021	-0.5	1342210175			
G051.7-1.0	51.7021	-1.0	1342210177			
G053.0+0.0	52.9787	0.0	1342210178			
G053.0+0.5	52.9787	0.5	1342210180			
G053.0+1.0	52.9787	1.0	1342210179			
G054.3+0.0	54.2553	0.0	1342210307			
G054.3-0.5	54.2553	-0.5	1342210308			
G054.3-1.0	54.2553	-1.0	1342210309			
G055.5+0.0	55.5319	0.0	1342210310			
G055.5+0.5	55.5319	0.5	1342210311			
G055.5+1.0	55.5319	1.0	1342210312			
G056.8+0.0	56.8085	0.0	1342210314			
G056.8-0.5	56.8085	-0.5	1342210315			
G056.8-1.0	56.8085	-1.0	1342210313			
G058.1+0.0	58.0851	0.0	1342210316			
G058.1+0.5	58.0851	0.5	1342210317			
G058.1+1.0	58.0851	1.0	1342210318			
G060.0+0.0	60.0000	0.0	1342210319			
G060.0-0.5	60.0000	-0.5	1342210320			
G060.0-1.0	60.0000	-1.0	1342210321			
G064.5+0.0	64.5283	0.0	1342210323			
G064.5+0.5	64.5283	0.5	1342210322			
G064.5+1.0	64.5283	1.0	1342210324			
G069.1+0.0	69.0566	0.0	1342210325			
G069.1-0.5	69.0566	-0.5	1342210326			
G069.1-1.0	69.0566	-1.0	1342210327			
G073.6+0.0	73.5849	0.0	1342210328			
G073.6+0.5	73.5849	0.5	1342210329			
G073.6+1.0	73.5849	1.0	1342210330			
G078.1+0.0	78.1132	0.0	1342210784			
G078.1-0.5	78.1132	-0.5	1342210787			
G078.1-1.0	78.1132	-1.0	1342220472			
G082.6+0.0	82.6415	0.0	1342197158			
G082.6+0.5	82.6415	0.5	1342199270			
G082.6+1.0	82.6415	1.0	1342199271			
G087.2+0.0	87.1698	0.0	1342197157			
G087.2-0.5	87.1698	-0.5	1342197156			
G087.2-1.0	87.1698	-1.0	1342197155			
G091.7+0.0	91.6981	0.0	1342197154			

LOS-ID	l(°)	b(°)	OBSID	OBSID	OBSID	OBSID
G091.7+1.0	91.6981	1.0	1342197153			
G091.7+2.0	91.7000	2.0	1342197152			
G096.2+0.0	96.2264	0.0	1342197150			
G096.2-1.0	96.2264	-1.0	1342197151			
G096.2-2.0	96.2000	-2.0	1342197149			
G109.8+0.0	109.8113	0.0	1342197148			
G109.8+1.0	109.8113	1.0	1342197147			
G109.8+2.0	109.8000	2.0	1342197146			
G114.3+0.0	114.3396	0.0	1342199276			
G114.3-1.0	114.3396	-1.0	1342199275			
G114.3-2.0	114.3000	-2.0	1342199277			
G127.9+0.0	127.9245	0.0	1342200751			
G127.9+1.0	127.9245	1.0	1342200750			
G127.9+2.0	127.9000	2.0	1342200749			
G132.5+0.0	132.4528	0.0	1342200748			
G132.5-1.0	132.4528	-1.0	1342200747			
G132.5-2.0	132.5000	-2.0	1342200746			
G146.0+0.0	146.0377	0.0	1342204529			
G146.0+1.0	146.0377	1.0	1342204530			
G146.0+2.0	146.0000	2.0	1342204528			
G150.6+0.0	150.5660	0.0	1342204532			
G150.6-1.0	150.5660	-1.0	1342204531			
G150.6-2.0	150.6000	-2.0	1342204533			
G164.2+0.0	164.1509	0.0	1342218053			
G164.2+1.0	164.1509	1.0	1342218051			
G164.2+2.0	164.2000	2.0	1342218052			
G168.7+0.0	168.6792	0.0	1342218049			
G168.7-1.0	168.6792	-1.0	1342218050			
G168.7-2.0	168.7000	-2.0	1342217686			
G184.5+0.0	184.5283	0.0	1342218516			
G184.5+1.0	184.5283	1.0	1342218515			
G184.5+2.0	184.5000	2.0	1342218514			
G189.1+0.0	189.0570	0.0	1342218517			
G189.1-1.0	189.0570	-1.0	1342218518			
G189.1-2.0	189.1000	-2.0	1342218519			
G202.6+0.0	202.6420	0.0	1342219313			
G202.6+1.0	202.6420	1.0	1342219314			
G202.6+2.0	202.6000	2.0	1342219315			
G207.2+0.0	207.1700	0.0	1342219311			
G207.2-1.0	207.1700	-1.0	1342219312			

LOS-ID	l(°)	b(°)	OBSID	OBSID	OBSID	OBSID
G207.2-2.0	207.2000	-2.0	1342219310			
G220.8+0.0	220.7550	0.0	1342220479			
G220.8+1.0	220.7550	1.0	1342220480			
G220.8+2.0	220.8000	2.0	1342220478			
G225.3+0.0	225.2830	0.0	1342220482			
G225.3-1.0	225.2830	-1.0	1342220481			
G225.3-2.0	225.3000	-2.0	1342204790			
G238.9+0.0	238.8680	0.0	1342220484			
G238.9+1.0	238.8680	1.0	1342220483			
G238.9+2.0	238.9000	2.0	1342220485			
G243.4+0.0	243.3960	0.0	1342204792			
G243.4-1.0	243.3960	-1.0	1342210298			
G243.4-2.0	243.3960	-2.0	1342204791			
G252.5+0.0	252.4530	0.0	1342210301			
G252.5-1.0	252.4530	-1.0	1342210302			
G257.0+0.0	256.9810	0.0	1342198393			
G257.0+1.0	256.9810	1.0	1342198392			
G261.4-2.0	261.4000	-2.0	1342198384			
G261.5+0.0	261.5090	0.0	1342198377			
G261.5-0.5	261.5090	-0.5	1342198378			
G261.5-1.0	261.5090	-1.0	1342198379			
G265.5-2.0	265.5000	-2.0	1342220486			
G266.0+0.0	266.0380	0.0	1342198376			
G266.0+1.0	266.0380	1.0	1342198375			
G266.0+2.0	266.0000	2.0	1342198374			
G270.6+0.0	270.5660	0.0	1342198371			
G270.6-1.0	270.5660	-1.0	1342198372			
G270.6-2.0	270.6000	-2.0	1342198373			
G275.1+0.0	275.0940	0.0	1342198370			
G275.1+0.5	275.0940	0.5	1342198369			
G275.1+1.0	275.0940	1.0	1342198368			
G279.6+0.0	279.6230	0.0	1342198365			
G279.6-0.5	279.6230	-0.5	1342198366			
G279.6-1.0	279.6230	-1.0	1342198367			
G284.2+0.0	284.1510	0.0	1342198364			
G284.2+0.5	284.1510	0.5	1342198363			
G284.2+1.0	284.1510	1.0	1342198362			
G288.7+0.0	288.6790	0.0	1342200740			
G288.7-0.5	288.6790	-0.5	1342200741			
G288.7-1.0	288.6790	-1.0	1342200742			

LOS-ID	l(°)	b(°)	OBSID	OBSID	OBSID	OBSID
G293.2+0.0	293.2080	0.0	1342200737			
G293.2+0.5	293.2080	0.5	1342200738			
G293.2+1.0	293.2080	1.0	1342200739			
G300.0+0.0	300.0000	0.0	1342200734			
G300.0-0.5	300.0000	-0.5	1342200735			
G300.0-1.0	300.0000	-1.0	1342200736			
G301.3+0.0	301.2770	0.0	1342200733			
G301.3+0.5	301.2770	0.5	1342200731			
G301.3+1.0	301.2770	1.0	1342200732			
G302.6+0.0	302.5530	0.0	1342200728			
G302.6-0.5	302.5530	-0.5	1342200729			
G302.6-1.0	302.5530	-1.0	1342200730			
G303.8+0.0	303.8300	0.0	1342200725			
G303.8+0.5	303.8300	0.5	1342200726			
G303.8+1.0	303.8300	1.0	1342200727			
G305.1+0.0	305.1060	0.0	1342201656			
G305.1-0.5	305.1060	-0.5	1342201657			
G305.1-1.0	305.1060	-1.0	1342201658			
G306.4+0.0	306.3830	0.0	1342201649			
G306.4+0.5	306.3830	0.5	1342201648			
G306.4+1.0	306.3830	1.0	1342201647			
G307.7+0.0	307.6600	0.0	1342201653			
G307.7-0.5	307.6600	-0.5	1342201654			
G307.7-1.0	307.6600	-1.0	1342201655			
G308.9+0.0	308.9360	0.0	1342201650			
G308.9+0.5	308.9360	0.5	1342201651			
G308.9+1.0	308.9360	1.0	1342201652			
G310.2+0.0	310.2130	0.0	1342201821			
G310.2-0.5	310.2130	-0.5	1342201822			
G310.2-1.0	310.2130	-1.0	1342201823			
G311.5+0.0	311.4890	0.0	1342201826			
G311.5+0.5	311.4890	0.5	1342201825			
G311.5+1.0	311.4890	1.0	1342201824			
G312.8+0.0	312.7660	0.0	1342201827			
G312.8-0.5	312.7660	-0.5	1342201828			
G312.8-1.0	312.7660	-1.0	1342201829			
G314.0+0.0	314.0430	0.0	1342201832			
G314.0+0.5	314.0430	0.5	1342201831			
G314.0+1.0	314.0430	1.0	1342201830			
G315.3+0.0	315.3190	0.0	1342201833			

LOS-ID	l(°)	b(°)	OBSID	OBSID	OBSID	OBSID
G315.3-0.5	315.3190	-0.5	1342201834			
G315.3-1.0	315.3190	-1.0	1342201835			
G316.6+0.0	316.5960	0.0	1342213719			
G316.6+0.5	316.5960	0.5	1342213701			
G316.6+1.0	316.5960	1.0	1342213718			
G317.9+0.0	317.8720	0.0	1342205699			
G317.9-0.5	317.8720	-0.5	1342205700			
G317.9-1.0	317.8720	-1.0	1342205701			
G319.1+0.0	319.1490	0.0	1342213699			
G319.1+0.5	319.1490	0.5	1342213700			
G319.1+1.0	319.1490	1.0	1342213337			
G320.4+0.0	320.4250	0.0	1342205702			
G320.4-0.5	320.4250	-0.5	1342205703			
G320.4-1.0	320.4250	-1.0	1342205704			
G321.7+0.0	321.7020	0.0	1342213720			
G321.7+0.5	321.7020	0.5	1342213336			
G321.7+1.0	321.7020	1.0	1342213698			
G323.0+0.0	322.9790	0.0	1342205705			
G323.0-0.5	322.9790	-0.5	1342205706			
G323.0-1.0	322.9790	-1.0	1342205707			
G324.3+0.0	324.2550	0.0	1342213721			
G324.3+0.5	324.2550	0.5	1342213722			
G324.3+1.0	324.2550	1.0	1342213723			
G325.5+0.0	325.5320	0.0	1342205757			
G325.5-0.5	325.5320	-0.5	1342205758			
G325.5-1.0	325.5320	-1.0	1342205756			
G326.8+0.0	326.8080	0.0	1342205710			
G326.8+0.5	326.8080	0.5	1342205709			
G326.8+1.0	326.8080	1.0	1342205708			
G328.1+0.0	328.0850	0.0	1342205753	1342205752		
G328.1-0.5	328.0850	-0.5	1342205754			
G328.1-1.0	328.0850	-1.0	1342205755			
G330.0+0.0	330.0000	0.0	1342205713			
G330.0+0.5	330.0000	0.5	1342205712			
G330.0+1.0	330.0000	1.0	1342205711			
G330.9+0.0	330.8700	0.0	1342205749	1342205748		
G330.9-0.5	330.8700	-0.5	1342205751			
G330.9-1.0	330.8700	-1.0	1342205750			
G331.7+0.0	331.7390	0.0	1342205716			
G331.7+0.5	331.7390	0.5	1342205715			

LOS-ID	l(°)	b(°)	OBSID	OBSID	OBSID	OBSID
G331.7+1.0	331.7390	1.0	1342205714			
G332.6+0.0	332.6090	0.0	1342205745	1342205744		
G332.6-0.5	332.6090	-0.5	1342205746			
G332.6-1.0	332.6090	-1.0	1342205747			
G333.5+0.0	333.4780	0.0	1342205719			
G333.5+0.5	333.4780	0.5	1342205718			
G333.5+1.0	333.4780	1.0	1342205717			
G334.3+0.0	334.3480	0.0	1342205743			
G334.3-0.5	334.3480	-0.5	1342205742			
G334.3-1.0	334.3480	-1.0	1342205741			
G335.2+0.0	335.2170	0.0	1342205722			
G335.2+0.5	335.2170	0.5	1342205721			
G335.2+1.0	335.2170	1.0	1342205720			
G336.1+0.0	336.0870	0.0	1342205740			
G336.1-0.5	336.0870	-0.5	1342205739			
G336.1-1.0	336.0870	-1.0	1342205738			
G337.0+0.0	336.9570	0.0	1342205725			
G337.0+0.5	336.9570	0.5	1342205724			
G337.0+1.0	336.9570	1.0	1342205723			
G337.8+0.0	337.8260	0.0	1342205735	1342205734		
G337.8-0.5	337.8260	-0.5	1342205736			
G337.8-1.0	337.8260	-1.0	1342205737			
G338.7+0.0	338.6960	0.0	1342205727	1342205726		
G338.7+0.5	338.6960	0.5	1342205728			
G338.7+1.0	338.6960	1.0	1342205729			
G339.6+0.0	339.5650	0.0	1342205829	1342205828		
G339.6-0.5	339.5650	-0.5	1342205830			
G339.6-1.0	339.5650	-1.0	1342205831			
G340.4+0.0	340.4350	0.0	1342205731	1342205730		
G340.4+0.5	340.4350	0.5	1342205732			
G340.4+1.0	340.4350	1.0	1342205733			
G341.3+0.0	341.3040	0.0	1342205825	1342205824		
G341.3-0.5	341.3040	-0.5	1342205826			
G341.3-1.0	341.3040	-1.0	1342205827			
G342.2+0.0	342.1740	0.0	1342205767	1342205766		
G342.2+0.5	342.1740	0.5	1342205768			
G342.2+1.0	342.1740	1.0	1342205769			
G343.0+0.0	343.0430	0.0	1342205821	1342205820		
G343.0-0.5	343.0430	-0.5	1342205822			
G343.0-1.0	343.0430	-1.0	1342205823			

LOS-ID	l(°)	b(°)	OBSID	OBSID	OBSID	OBSID
G343.9+0.0	343.9130	0.0	1342205771	1342205770		
G343.9+0.5	343.9130	0.5	1342205772			
G343.9+1.0	343.9130	1.0	1342205773			
G344.8+0.0	344.7830	0.0	1342205817	1342205816		
G344.8-0.5	344.7830	-0.5	1342205818			
G344.8-1.0	344.7830	-1.0	1342205819			
G345.7+0.0	345.6520	0.0	1342205775	1342205774		
G345.7+0.5	345.6520	0.5	1342205776			
G345.7+1.0	345.6520	1.0	1342205777			
G346.5+0.0	346.5220	0.0	1342205813	1342205812		
G346.5-0.5	346.5220	-0.5	1342205814			
G346.5-1.0	346.5220	-1.0	1342205815			
G347.4+0.0	347.3910	0.0	1342205779	1342205778		
G347.4+0.5	347.3910	0.5	1342205780			
G347.4+1.0	347.3910	1.0	1342205781			
G348.3+0.0	348.2610	0.0	1342205809	1342205808		
G348.3-0.5	348.2610	-0.5	1342205810			
G348.3-1.0	348.2610	-1.0	1342205811			
G349.1+0.0	349.1300	0.0	1342205783	1342205782		
G349.1+0.5	349.1300	0.5	1342205784			
G349.1+1.0	349.1300	1.0	1342205785			
G350.0+0.0	350.0000	0.0	1342205805	1342205804		
G350.0-0.5	350.0000	-0.5	1342205806			
G350.0-1.0	350.0000	-1.0	1342205807			
G350.9+0.0	350.8700	0.0	1342205787	1342205786		
G350.9+0.5	350.8700	0.5	1342205788			
G350.9+1.0	350.8700	1.0	1342205789			
G351.7+0.0	351.7390	0.0	1342205800			
G351.7-0.5	351.7390	-0.5	1342205801			
G351.7-1.0	351.7390	-1.0	1342205802			
G352.6+0.0	352.6090	0.0	1342205790			
G352.6+0.5	352.6090	0.5	1342205791			
G352.6+1.0	352.6090	1.0	1342205792			
G353.5+0.0	353.4780	0.0	1342206398			
G353.5-0.5	353.4780	-0.5	1342206399			
G353.5-1.0	353.4780	-1.0	1342216743			
G354.3+0.0	354.3480	0.0	1342214495			
G354.3+0.5	354.3480	0.5	1342206397			
G354.3+1.0	354.3480	1.0	1342206396			
G355.2+0.0	355.2170	0.0	1342216746			

LOS-ID	l(°)	b(°)	OBSID	OBSID	OBSID	OBSID
G355.2-0.5	355.2170	-0.5	1342216745			
G355.2-1.0	355.2170	-1.0	1342216744			
G356.1+0.0	356.0870	0.0	1342214494			
G356.1+0.5	356.0870	0.5	1342214493			
G356.1+1.0	356.0870	1.0	1342214492			
G357.0+0.0	356.9570	0.0	1342214490	1342214489		
G357.0-0.5	356.9570	-0.5	1342214488	1342214487		
G357.0-1.0	356.9570	-1.0	1342216747	1342214486		
G357.8+0.0	357.8260	0.0	1342214481	1342214480		
G357.8+0.5	357.8260	0.5	1342214483	1342214482		
G357.8+1.0	357.8260	1.0	1342214485	1342214484		
G358.7+0.0	358.6960	0.0	1342216766	1342216765		
G358.7+0.5	358.6960	0.5	1342216787	1342214479		
G358.7-0.5	358.6960	-0.5	1342216768	1342216767		
G358.7+1.0	358.6960	1.0	1342216782	1342214478		
G358.7-1.0	358.6960	-1.0	1342216764	1342216763		
G359.5+0.0	359.5000	0.0	1342216786	1342216785	1342216781	1342216779

Table 2
Summary of Data Used for the Position-Velocity FITS Image Data

Target Name	Direction	center (l^o,b^o)	length (arcmin)	OBSID	LOF**
CII_G0.0+0.2-1	latitude	(0.0,0.2)	24	1342214476	LOF1
CII_G0.0+0.2-1	latitude	(0.0,0.2)	24	1342214477	LOF2
CII_G0.0+0.6-1	latitude	(0.0,0.6)	24	1342216770	LOF2
CII_G0.0+0.6-1	latitude	(0.0,0.6)	24	1342216783	LOF1
CII_G000.0-0.2-1	latitude	(0.0,-0.2)	24	1342216759	LOF1
CII_G000.0-0.2-1	latitude	(0.0,-0.2)	24	1342216761	LOF2
CII_G000.0-0.6-1	latitude	(0.0,-0.6)	24	1342216758	LOF1
CII_G000.0-0.6-1	latitude	(0.0,-0.6)	24	1342216760	LOF2
CII_G000.2+0.0-1	longitude	(0.2,0.0)	24	1342216771	LOF2
CII_G000.2+0.0-1	longitude	(0.2,0.0)	24	1342216792	LOF1
CII_G000.6+0.0-1	longitude	(0.6,0.0)	24	1342216755	LOF1
CII_G000.6+0.0-1	longitude	(0.6,0.0)	24	1342216756	LOF2
CII_G359.4+0.0-1	longitude	(359.4,0.0)	24	1342216757	LOF2
CII_G359.4+0.0-1	longitude	(359.4,0.0)	24	1342216762	LOF1
CII_G359.8+0.0-1	longitude	(359.8,0.0)	24	1342216769	LOF1
CII_G359.8+0.0-1	longitude	(359.8,0.0)	24	1342216793	LOF2

** Each OTF scan center was observed in two LO setting to cover the broader range of velocities characteristic of the CMZ. The LO values in the AORs are LOF1=1896.53 GHz and LOF2 = 1897.48 GHz, whereas the actual observed LO values (in the headers) may differ slightly.